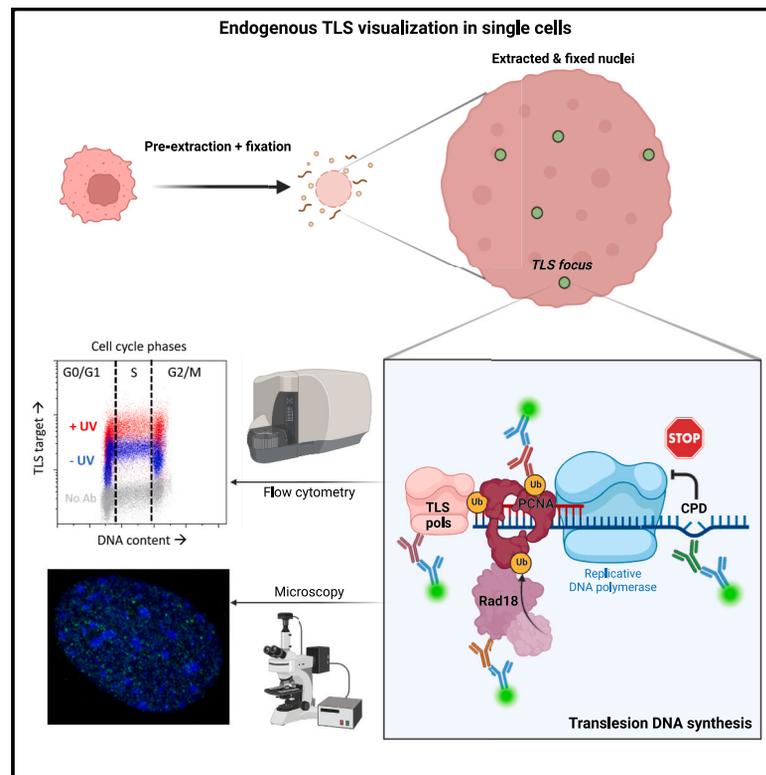**Article**

Detection of endogenous translesion DNA synthesis in single mammalian cells

Graphical abstract

Authors

Tom Egger, Antoine Aze,
Domenico Maiorano

Correspondence

domenico.maiorano@igh.cnrs.fr

In brief

The DNA damage tolerance pathway involving translesion DNA synthesis (TLS) allows cells to proliferate in the presence of DNA lesions and is widely studied in the context of cancer. Detection of TLS factors has often relied on ectopically tagged proteins. Here, Egger and colleagues report methods for analyzing endogenous TLS in single cells by flow cytometry and immunofluorescence.

Highlights

- Tools for monitoring endogenous translesion synthesis (TLS) factors

- Detection of endogenous PCNA^{mUb} and Y-family TLS pols in single mammalian cells

- Monitoring chromatin-bound TLS factors during cell cycle phases

- PCNA^{mUb} and not TLS polη co-localizes with sites of replication forks stalled by CPDs

CelPress

Article

Detection of endogenous translesion DNA synthesis in single mammalian cells

Tom Egger,[1,2] Antoine Aze,[1] and Domenico Maiorano[1,3,*]
[1]Institut de Génétique Humaine (IGH) CNRS UMR9002, Université de Montpellier, Molecular Bases of Human Pathologies Department, "Genome Surveillance and Stability" Laboratory, 34396 Cedex 5 Montpellier, France
[2]Present address: "Genome Instability and Cancer" Laboratory, 34396 Cedex 5 Montpellier, France
[3]Lead contact
*Correspondence: domenico.maiorano@igh.cnrs.fr
https://doi.org/10.1016/j.crmeth.2023.100501

MOTIVATION Detection of chromatin-bound TLS factors in single cells, such as PCNA^{mUb} and TLS pols, has typically depended on either western blotting or detection of ectopically expressed, tagged proteins. Western blotting has the limitation of only providing information on the average level of proteins in a cell population, while localization studies using ectopically expressed, tagged proteins may not faithfully represent the behavior of endogenous proteins. We help to address this problem by developing flow cytometry and immunofluorescence methods to detect endogenous, chromatin-bound PCNA^{mUb} as well as Y-family TLS pols in single mammalian cells. We applied these methods to study DNA replication and TLS dynamics in HCT116 colon cancer cells exposed to UV-C irradiation and provide evidence for uncoupling of PCNA^{mUb} from Polη-dependent TLS at replication forks stalled by UV-C lesions.

SUMMARY

Translesion DNA synthesis (TLS) is an evolutionarily conserved process that cells activate to tolerate DNA damage. TLS facilitates proliferation under DNA damage conditions and is exploited by cancer cells to gain therapy resistance. It has been so far challenging to analyze endogenous TLS factors such as PCNA^{mUb} and TLS DNA polymerases in single mammalian cells due to a lack of suitable detection tools. We have adapted a flow cytometry-based quantitative method allowing detection of endogenous, chromatin-bound TLS factors in single mammalian cells, either untreated or exposed to DNA-damaging agents. This high-throughput procedure is quantitative, accurate, and allows unbiased analysis of TLS factors' recruitment to chromatin, as well as occurrence of DNA lesions with respect to the cell cycle. We also demonstrate detection of endogenous TLS factors by immunofluorescence microscopy and provide insights into TLS dynamics upon DNA replication forks stalled by UV-C-induced DNA damage.

INTRODUCTION

Translesion synthesis (TLS) constitutes a branch of the cellular DNA damage tolerance pathway involving DNA lesions bypassed by specialized DNA polymerases, known as TLS pols. Thanks to a catalytic site that is more open than that of replicative DNA polymerases, these enzymes can accommodate damaged DNA bases and facilitate DNA replication under DNA damage conditions. However, TLS pols have lower fidelity than replicative DNA polymerases and are therefore mutagenic.[1] By facilitating proliferation under DNA damage and increasing genetic diversity, TLS is exploited by cancer cells to adapt to therapy, thus escaping apoptosis, and has recently drawn much attention as a pathway to target so as to sensitize cancer cells to therapy.[2,3] Y-family TLS pols (η, ι, κ, and Rev1) are implicated in rescuing replication forks arrested by DNA damage. Their recruitment onto DNA lesions pri-

marily depends upon monoubiquitination of the replication-associated protein PCNA (PCNA^{mUb}), catalyzed by the Rad6(E2)/Rad18(E3) ubiquitin ligase complex,[4,5] and is dependent upon formation of excess single-stranded (ss)DNA produced by enzymatic uncoupling of replication forks stalled by DNA lesions.[6,7] So far, it has been difficult to study endogenous PCNA^{mUb} and TLS pols recruitment due to a lack of specific tools and detection methods in single cells. In particular, detection of endogenous nuclear PCNA^{mUb} in single cells by immunostaining has been challenging mainly due to the lack of a specific antibody to detect PCNA^{mUb}. Ectopically expressed PCNA^{mUb} was previously detected in chicken DT40 cells by fluorescence resonance energy transfer (FRET), using a fluorescently tagged version of both ubiquitin and PCNA.[8] Although PCNA^{mUb} and TLS pols recruitment can be analyzed by western blotting in total or nuclear extracts, this rather crude method only provides an indication of the

average level of recruitment in a large number of cells. Further, this method can be difficult to apply in cell lines that are sensitive to the extraction procedure. Furthermore, analysis of their recruitment in respect to the cell cycle involves synchronization procedures that can induce bias in the interpretation of the experiment. It has also been challenging to analyze recruitment of endogenous Y-family TLS pols onto damaged chromatin in single cells, presumably because of their low expression level. Current methods involve ectopic expression of epitope-tagged versions, such as fluorescent proteins, followed by detection of natural fluorescence in live or fixed cells.[9–13] These methods can also induce bias since they involve TLS pols overexpression. In addition, the presence of the tag may affect the chromatin-binding affinity of the protein under study. Finally, upon transfection, the level of ectopically expressed TLS pols can be variable from cell to cell.

With this in mind, we sought to develop a procedure to visualize endogenous PCNA[mUb] as well as Y-family TLS pols in single cells by both flow cytometry and immunofluorescence. The quantitative cytometry-based method described here is simple: it allows monitoring of the dynamics of PCNA[mUb] and TLS pols, as well as that of Rad18 in individual cells in a quantitative fashion and requires fewer cells than in western blot. Using this method, TLS pols recruitment to chromatin can be analyzed in a cell population with great accuracy and in relation to the cell cycle phases. TLS factors binding to chromatin can be analyzed quantitatively and with respect to DNA lesions, DNA damage markers, and DNA synthesis. We have also applied this procedure to visualize both endogenous PCNA[mUb] and TLS pols bound to chromatin by immunofluorescence and show that PCNA[mUb] and TLS pols can be detected in single untreated cells or following exposure to DNA-damaging agents.

RESULTS

Detection of endogenous PCNA[mUb] by flow cytometry

We modified a protocol from a previous method employed to detect chromatin-bound RPA by flow cytometry,[14] to allow detection of poorly expressed, loosely chromatin-bound proteins, such as PCNA[mUb] and TLS pols. In this procedure, cells are briefly pre-extracted with detergent, before their rapid fixation, so as to freeze them in their natural position within the cell cycle. We optimized the detection of chromatin-bound PCNA[mUb] by trying various combinations of detergent-based pre-extraction and fixation steps (STAR Methods; Figures S1A–S1D). Using an antibody that specifically recognizes PCNA[mUb] in western blot (Figure S1E; Thakar et al.,[15] Swain et al.,[16] and Despras et al.[17]), we could detect chromatin-bound PCNA[mUb] by flow cytometry, which, in this assay, is scored as an increase of the fluorescence signal compared with the background signal of the control sample (no antibody; Figure 1A). PCNA[mUb] chromatin binding was observed in untreated HCT116 colon cancer cells, which further increased upon exposure to genotoxic doses of either UV-C irradiation or hydrogen peroxide (H₂O₂), but not to camptothecin (CPT) as expected (Figures 1A and S1F), because CPT generates mainly DNA double-strand breaks and limited ssDNA (Recolin et al.,[18] for review). Consistent with this notion, upon exposure to UV light, the increase in PCNA[mUb] fluorescence correlated with an increase in RPA fluorescence (Figure S2A), supporting previous observa-

tions.[14,19] In parallel, PCNA[mUb] chromatin binding was confirmed by analysis of cellular fractions by western blot (Figure S2B). As expected, Rad18 downregulation by small interfering RNA (siRNA) decreased PCNA[mUb] fluorescence in two different UV-irradiated cell lines, as expected (Figure S2C). A similar result was obtained upon expression of a PCNA mutant that cannot be monoubiquitinated (K164R; Figure S2D), demonstrating the specificity of the signal. Further, upon exposure to UV light, a specific increase in PCNA[mUb] fluorescence and not total PCNA, whose level remained unchanged, was observed (Figures S2E and S2F). By plotting the integrated PCNA[mUb] fluorescence intensity against that of DAPI (DNA content), PCNA[mUb] chromatin binding could be further scored in relation to cell cycle (Figure 1B). After UV irradiation, PCNA[mUb] increased in all cell cycle phases, while it was mainly restricted to G1 and G2/M phases upon exposure to H₂O₂ (Figure 1B). Analysis of PCNA[mUb] by both western blot and flow cytometry during a time course following exposure to UV radiation shows a tight correlation between the two methods (Figures 1C–1E). Western blot analysis shows an increase in the total level of PCNA[mUb] with time, reaching a maximum at 8.5 h after irradiation in this experiment (Figure 1C). A very similar increase was also seen by flow cytometry (Figure 1D), and the kinetics of the two detection methods very closely overlapped (Figure 1E). PCNA[mUb] could also be detected by flow cytometry in other cell lines (Figure S3A), although at different levels. The intensity of PCNA[mUb] fluorescence correlated with both the amount of cells in S phase (Figure S3B) and PCNA[mUb] abundance, as determined by western blot (Figure S3C). Altogether, these results show that chromatin recruitment of PCNA[mUb] can be reliably detected by flow cytometry and can be correlated with the cell cycle stages where it occurs.

Detection of endogenous TLS pols by flow cytometry

We next applied the same protocol to detect chromatin recruitment of endogenous Y-family TLS pols by flow cytometry using specific antibodies validated in western blot (see STAR Methods and Figures S4A–S4C, S6C, and S6D). As can be seen in Figures 2A, 2B, and S5, we could detect chromatin binding of at least two TLS pols, Polη and Polι, as well as Rad18 (Figure 2C). Their association with chromatin was confirmed in parallel by western blotting (Figures S2B and S4C). Notwithstanding, differences in the fluorescence intensity were observed among TLS pols. In particular, upon UV irradiation, increased Polη and Polι fluorescence was clearly detectable, while this was much less evident for Polκ (Figure S5). Although these results are consistent with the notion that both Polη and Polι, and not Polκ, are involved in TLS of UV damage, at this stage, we cannot exclude that the observed differences are due to the relative abundance of TLS pols, the strength of the antibodies used, or both. Polη and Polι were found to be chromatin bound at all cell cycle stages, while Rad18 increased in a DNA replication-dependent manner (Figures 2C and S5). As for Rev1, we failed to detect a significant signal with currently available antibodies. At the same time, by flow cytometry, we could also clearly detect cyclobutane pyrimidine dimer (CPD) UV photoproducts, using a specific antibody (see STAR Methods), which were mainly distributed in the S phase upon UV irradiation (Figures 2D and S5). Importantly, we found that detection of different TLS factors by flow cytometry is strictly dependent upon the fixation method, which can be different for
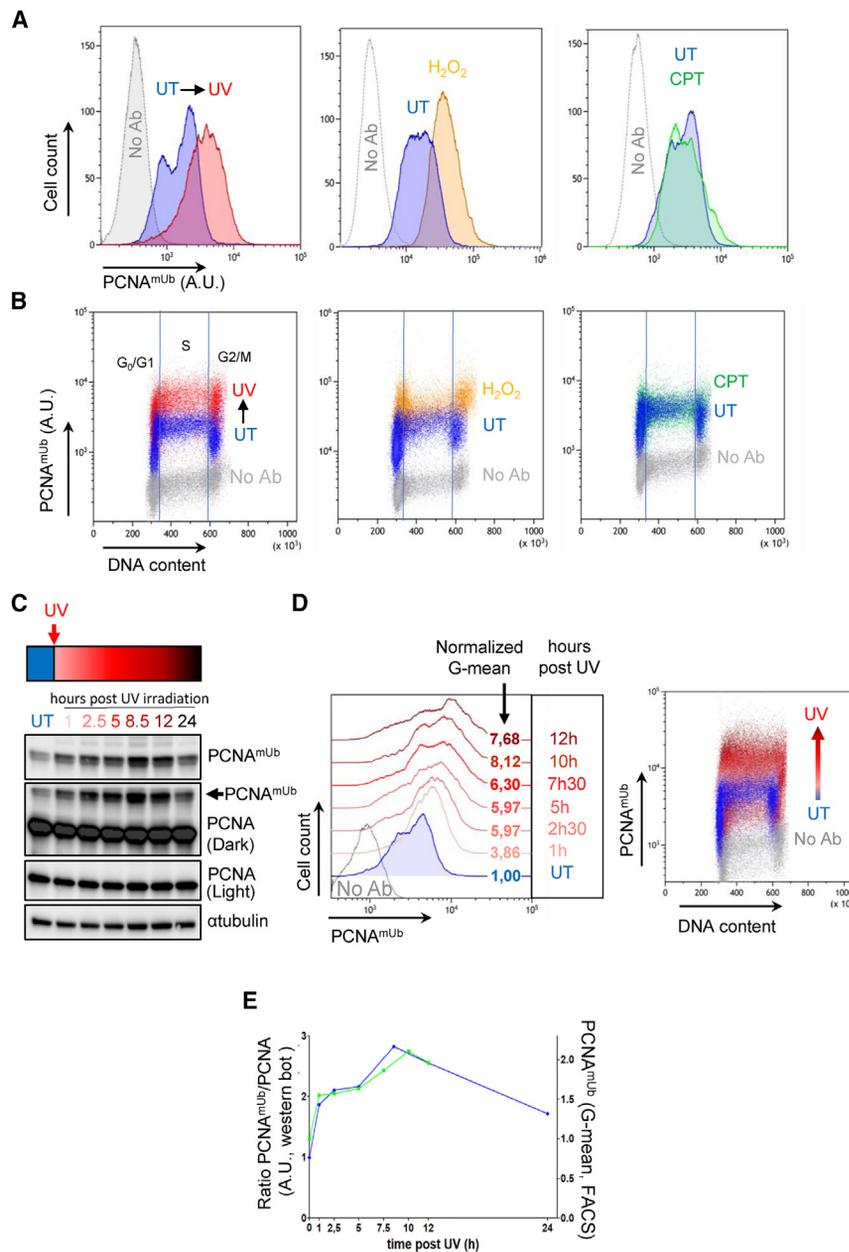
Figure 1. Detection of endogenous PCNA^{mUb} recruitment to chromatin by flow cytometry

(A) Detection of endogenous PCNA^{mUb} in HCT116 cells either untreated (UT, blue) or exposed to 20 J/m^2 of UV-C light (UV, red), 1 mM hydrogen peroxide (H$_2$O$_2$, orange), or 1 μM camptothecin (CPT, green) by flow cytometry. A sample devoid of primary antibody (No Ab) was included as a control. Data were plotted as PCNA^{mUb} fluorescence intensity versus the total cells count. A.U., arbitrary units. n = 3.

(B) In this panel, PCNA^{mUb} fluorescence intensity was plotted against the DAPI fluorescence that counterstains the DNA (DNA content), thus giving the cell cycle profile. n = 3.

(C and D) Time course of PCNA^{mUb} analyzed by either western blot (C) or flow cytometry (D) in HCT116 cells UT or exposed to 20 J/m^2 UV. Samples were taken at the indicated times after UV irradiation (red arrow). The increase in the deepness of the red color indicates the increase in time. Data of (D) are plotted as in (A) and (B). No Ab was included as a control. n = 2.

(E) Quantification of PCNA^{mUb} time courses of (C) and (D). The western blot signals of PCNA^{mUb} were normalized to the total PCNA level (blue line). The geometric mean (G-Mean) of cells computed by flow cytometry is plotted in green. n = 2.

upon Rad18 downregulation by siRNA (Figures 3A and 3B; STAR Methods) or upon expression of the *pcna^{K164R}* mutant that cannot be monoubiquitinated (Figure S6A). The PCNA^{mUb} background level persisting in cells treated by siRad18 could be either due to incomplete Rad18 depletion or to the activity of the CRL4^{Cdt2} (E3) ligase.[21] PCNA^{mUb} signal was detected as discrete nuclear foci, co-localizing with total PCNA even in untreated cells (Figure 3C), which likely represent PCNA^{mUb} induced by endogenous replication stress, consistent with the flow cytometry data shown in Figure 1. PCNA^{mUb} foci were co-localized with total PCNA (Figure 3C) and the ssDNA binding protein RPA (Figure 3D), in line with the notion that ssDNA is essential for PCNA^{mUb}, although not all RPA foci co-localized with PCNA^{mUb}, and vice versa. As expected, the intensity of both the PCNA^{mUb} and RPA fluorescence increased upon UV irradiation (Figure 3E). We also observed PCNA^{mUb} foci in cells treated with different DNA-damaging agents such as cisplatin and H$_2$O$_2$, but to a much lesser extent with CPT (Figures 4A and 4B), consistent with flow cytometry data (Figures 1A, 1B, and S1). Altogether, these results show that PCNA^{mUb} can be detected in single HCT116 cells by indirect immunofluorescence, enabling its observation at the sub-nuclear level and its co-localization with diverse factors implicated in DNA metabolism.
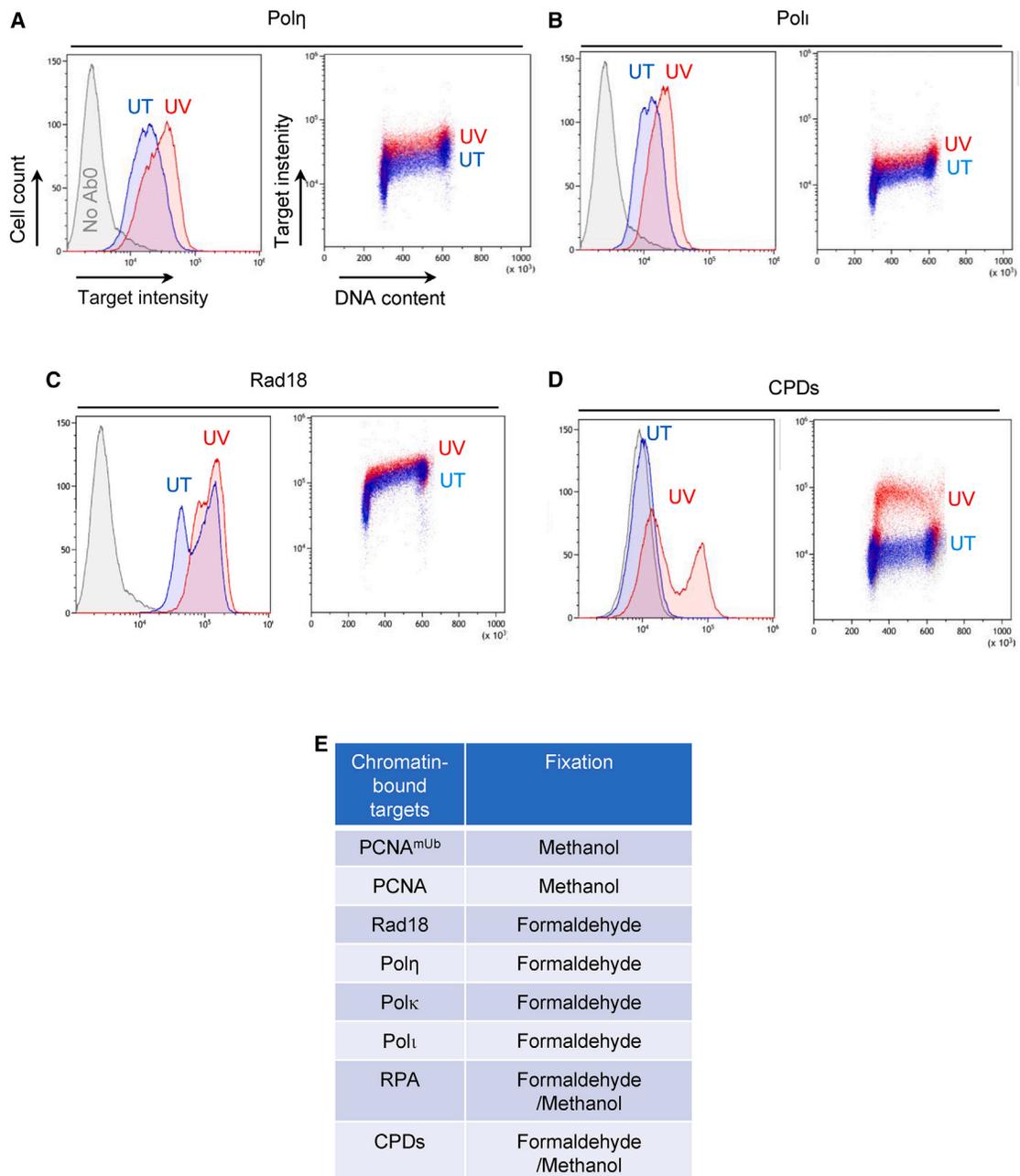
each protein target (Figure 2E). Altogether, these results show that at least two endogenous Y-family TLS pols can be detected by flow cytometry, as well as Rad18 and CPDs, and that their binding to chromatin can be observed in relation to the cell cycle in single cells without the use of synchronization methods.

Detection of nuclear PCNA^{mUb} by immunofluorescence in single cells

Using the same extraction and fixation procedure, we attempted to detect PCNA^{mUb} by indirect immunofluorescence in mammalian cells. We observed clear PCNA^{mUb} nuclear foci in untreated HCT116 cells that increased following exposure to UV radiation and whose extent was strongly reduced either

Figure 2. Detection of endogenous Rad18 and TLS pols chromatin recruitment by flow cytometry

(A–C) Detection of endogenous TLS pols (A and B) or Rad18 (C) in HCT116 cells either untreated (UT, blue) or exposed to 20 J/m^2 of UV-C light (UV, red) by flow cytometry. A sample devoid of primary antibody (No Ab) was included as a control. Data are plotted as in Figures 1A and 1B.
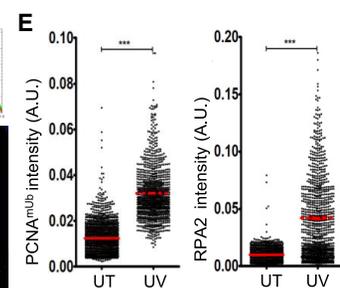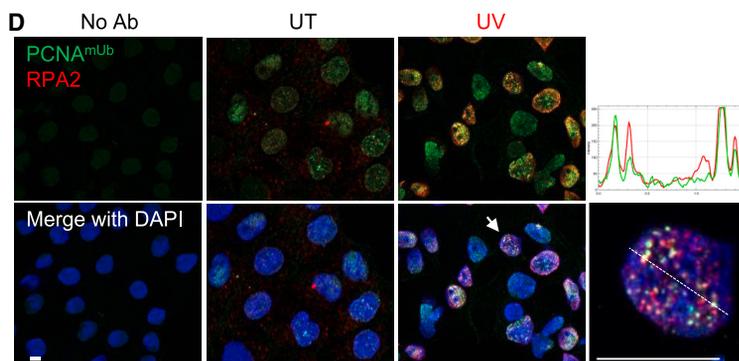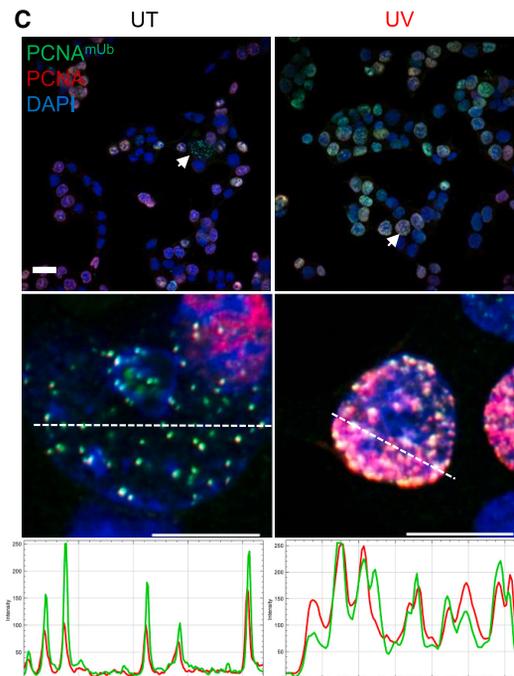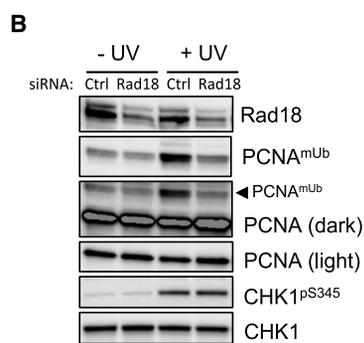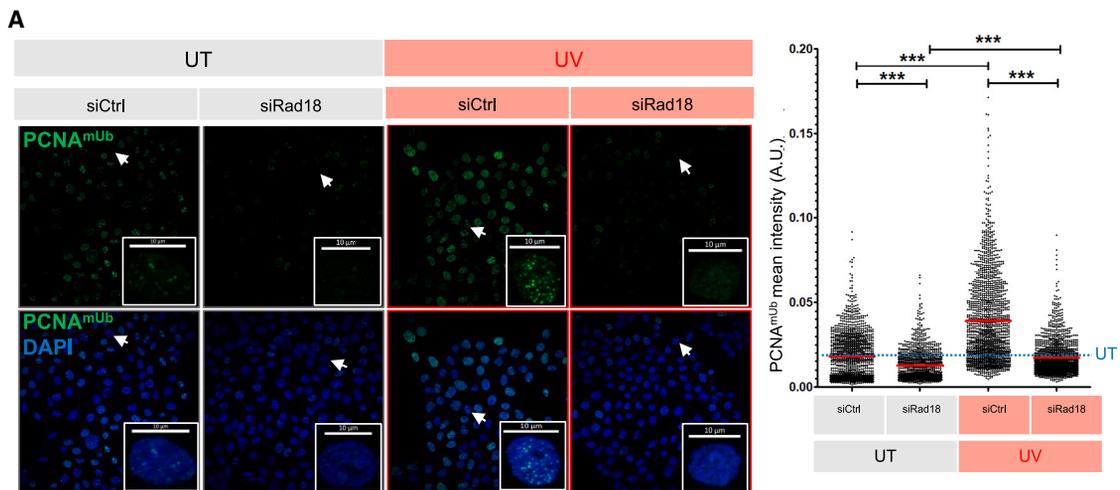
(D) Detection of UV-induced cyclobutane pyrimidine dimers (CPDs) by flow cytometry. No Ab was included as a control. Data are plotted as in Figures 1A and 1B.

(E) Table describing the different fixation methods to detect chromatin-bound proteins related to the TLS pathway in human cells. n = 3. For more details see Egger et al.[20]

Detection of chromatin-bound TLS Polη and Polι by immunofluorescence in single cells

As done for PCNA^{mUb}, we next attempted to detect Y-family TLS pols in single cells by indirect immunofluorescence. We were able to detect endogenous Polη (Figures 5A and 5B) and Polι

(Figure 5C) in nuclei of HCT116 cells. Polη was not detected in HCT116 cells upon downregulation by siRNA, nor in XP30RO fibroblasts harboring a homozygous mutation in the Polη gene (Figures S6C and S6D).[22] In contrast, Polη was detectable in XP30RO cells complemented with either wild-type Polη or

(legend on next page)

GFP-Polη.[13] In the latter, most of the Polη foci detected by the Polη antibody also co-localized with the GFP fluorescence, although a fraction of them did not. Equally, the Polι signal was strongly reduced upon inhibition of its expression by siRNA (Figure 5C), demonstrating the specificity of the signal. As a comparison, we also transfected HCT116 cells with EGFP-Polη. As can be seen in Figure 5B, detection of endogenous Polη by immunofluorescence gives a better and more comprehensive landscape of Polη distribution in isolated cells compared with ectopic transfection, which provides poor information and is limited to the fraction of cells that were successfully transfected. Detailed analysis of the fluorescence signals generated by the Polη antibody shows that endogenous Polη forms discrete nuclear foci in both untreated and UV-irradiated cells (Figure 5B), supporting two previous observations.[23,24] This is different from what has been observed in cells transfected with GFP-tagged Polη in which only a small fraction of the cells form nuclear foci in unperturbed conditions, while in the remaining population, the protein remains uniformly distributed in the cell.[13,25] Quantification shows that upon UV irradiation, or exposure to H₂O₂, the fluorescence intensity markedly increased, suggesting recruitment to damaged chromatin (Figure 5A). In conclusion, these results show that both endogenous TLS Polη and Polι can be detected by immunofluorescence in isolated mammalian cells.

Getting insights into TLS activation by UV damage during ongoing DNA synthesis

As an application of this procedure to study TLS dynamics in proliferating cells, we wished to analyze the localization of PCNA^mUb and Polη with respect to DNA lesions induced by UV irradiation (CPDs) and to sites of DNA synthesis. For this purpose, we exposed cells to UV light to generate DNA lesions, followed by a short pulse with the nucleotide analog EdU to label ongoing replication forks (Figure 6A). Cells were sampled post-UV irradiation and triple stained with antibodies for either PCNA^mUb (red, Figure 6) or Polη (red, Figure 7), EdU (green), and CPDs (blue). Figure 6B shows that in untreated (UT) cells, nuclear PCNA^mUb foci were visible in both EdU-negative cells, representing cells in either G1 or G2/M cell cycle phases, and in EdU-positive cells (green, S-phase cells), consistent with results obtained by flow cytometry (Figures 1A and 1B). Co-local-

ization of PCNA^mUb and EdU was already visible immediately after the EdU pulse (Figures 6C and 6E, t = 0) and increased shortly after (t = 0.5 h). White spots (merge of the three colors, see color table in Figure 6A) could also be clearly visible at this time point, showing co-localization of PCNA^mUb and EdU at sites of DNA lesions (CPDs; Figure 6E, right). With time, the intensity of the CPD and PCNA^mUb fluorescence increased, giving rise to a magenta color (merge of red and blue). Of note, CellProfiler quantification shows that the number of CPDs foci per nucleus decreased with time, while their intensity increased, suggesting clustering of CPD lesions (Figure S6E). Because the CPD signal intensity stalled at 2.5 h and only slightly decreased at 5 h, this suggested that CPD clustering might represent sites of active DNA repair (e.g., nucleotide excision repair, NER). In support of this possibility, proteins involved in NER have been previously observed forming discrete nuclear foci in mammalian cells.[26] Further, these kinetics are consistent with a previous study showing that CPDs are still relatively abundant 5 h after irradiation.[27] At later time points (2.5–5 h), the magenta color was predominant (merge of red and blue), indicating that PCNA^mUb was mostly located onto CPDs, moving away from EdU incorporation sites. These observations suggest that following UV irradiation, PCNA^mUb transiently co-localizes with sites of DNA synthesis stalled by UV-induced DNA lesions. CellProfiler quantification (Figure 6D) shows that PCNA^mUb occurred first in EdU-positive cells (EdU⁺; 0.5 to 1 h time point) while at later time points (2.5–5 h) EdU-negative cells (EdU⁻) also started to show increased PCNA^mUb. These latter events may correspond to G1 cells entering into S phase in the presence of UV-induced DNA lesions since PCNA^mUb increased during replication of both untreated and UV-irradiated cells (Figure 1B).

As for Polη, the picture was surprisingly different (Figure 7). Consistent with flow cytometry data (Figure 2), Polη foci could be observed in untreated cells that were not co-localizing with sites of ongoing DNA synthesis (Figures 7B–7D, EdU, green) but were close to them (white arrows). At early time points post-UV irradiation (t = 0.5 h), and in contrast to PCNA^mUb foci, Polη foci were still observed close to EdU foci but not completely overlapping. At later time points (1–5 h), Polη foci were close but clearly separated from EdU foci, with only rare foci showing co-localization. Notably, 1 h post-UV irradiation, Polη foci were

---

Figure 3. Detection of nuclear PCNA^mUb in single cells by immunofluorescence

(A) HCT116 cells untreated (UT), or exposed to 20 J/m² of UV-C (UV, red), treated with either siRNA control (siCtrl) or an siRNA targeting Rad18 (siRad18). Cells were stained with the PCNA^mUb antibody and visualized by indirect immunofluorescence. DNA was counterstained with DAPI. Insets: magnification of single cells (indicated by a white arrow). Right: quantification of PCNA^mUb foci with CellProfiler software (see STAR Methods). A.U., arbitrary units. Stars indicate significant differences, ***p < 0.001 (non-parametric Mann Whitney test). n = 3.

(B) Western blot of HCT116 cells of the experiment shown in (A), treated with the indicated siRNA, exposed (+UV) or not (−UV) to 20 J/m² of UV-C. Proteins were detected with the indicated antibodies. The anti-PCNA antibody detects both unmodified and PCNA^mUb, n = 3.

(C) Top: HCT116 cells UT or exposed to UV-C (UV) were co-stained with both PCNA^mUb and total PCNA and viewed by indirect immunofluorescence. DNA was visualized with DAPI. Middle: magnification of a nucleus from a single cell of each panel (indicated by a white arrow). Cross-sections were drawn with Zen Blue software to quantify the co-localized relative intensities of PCNA^mUb (green) and PCNA (red) fluorescence. Bottom: quantification of the relative intensity of the cross-section for both PCNA and PCNA^mUb labeling of each nucleus of the middle panel. n = 2. Scale bar: 10 μm.

(D) HCT116 cells UT or exposed to UV-C (UV) were co-stained with both PCNA^mUb and RPA2 antibodies and viewed by indirect immunofluorescence. DNA was visualized with DAPI. Far top right: quantification of the relative intensity of the cross-section here below for both PCNA and RPA2 labeling of the nucleus indicated by a white arrow. The cross-section was drawn with ImageJ software to visualize co-localization of PCNA^mUb (green) with RPA2 (red) fluorescence. n = 2. Scale bar: 10 μm.

(E) Quantification of either PCNA^mUb (left) or RPA2 (right) of experiment shown in (D). Stars indicate significant differences, ***p < 0.001. ns, non-significant (non-parametric Mann Whitney test).
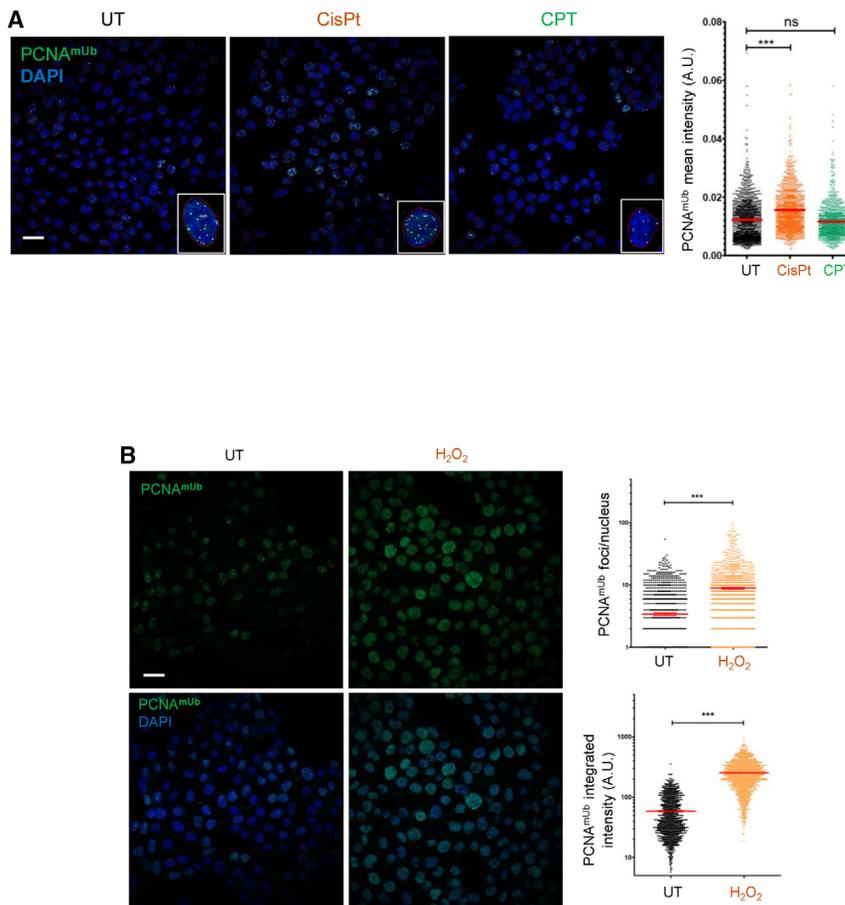
Figure 4. PCNA^mUb detection by immunofluorescence in HCT116 cells exposed to different DNA-damaging agents

(A) Left: wide-field images of HCT116 cells untreated (UT) or exposed to either 30 μM cisplatin (CisPt) or 1 μM camptothecin (CPT) stained with the anti-PCNA^mUb antibody and counterstained with DAPI to visualize nuclei. Insets: magnification of individual nuclei. Right: quantification of PCNA^mUb immunofluorescence mean intensity of nuclei assessed with CellProfiler. Scale bar: 20 μm. n = 2.

(B) Left: wide-field images of HCT116 cells UT or exposed to hydrogen peroxide (H_2O_2), stained with the anti-PCNA^mUb antibody and counterstained with DAPI to visualize nuclei. Right: quantification of PCNA^mUb of the left panel. Scale bar: 20 μm. n = 2.

mized detection protocol. This simple and fast method now makes it possible to analyze endogenous TLS in single cells without the use of synchronization procedures that would introduce bias in the analysis of the results.

Results obtained in this article show that, upon exposure of HCT116 cells to DNA-damaging agents, recruitment of both PCNA^mUb and TLS pols onto chromatin occurs in all cell cycle phases, although mainly in S phase and with some important differences depending on the type of DNA damage. In cells exposed to UV radiation, PCNA^mUb chromatin binding was detected in all cell cycle stages, with a slight increase in G1 and G2/M phases. A similar pattern was observed for at least two Y-family TLS pols (η and ι). These observations are consistent with the notion that UV-induced DNA lesions stall replication forks and that TLS can also occurs outside S phase.[25,28–32] When cells were treated with H_2O_2, the pattern of PCNA^mUb fluorescence observed by flow cytometry was rather different, being more restricted to the G1 and G2/M phases. This result can be explained by the observation that 8-oxodG, the main DNA lesion generated by H_2O_2, does not interfere much with replicative polymerases[33] and therefore limits the extent of PCNA^mUb in S phase. These lesions are actively repaired by a base excision repair-based process, leading to formation of a gapped ssDNA intermediate that stimulates PCNA^mUb. Notwithstanding, different observations were reported about the cell cycle phase when the gap filling process occurs,[28,29] which could be explained by the use of a different cell line and different methods of cell synchronization. The non-invasive and quantitative method presented here provides a clear picture, showing that in cells treated with H_2O_2, PCNA^mUb occurs mainly in G1, in line with an early report,[31] but can also occur in S phase.

Observation of PCNA^mUb by immunofluorescence shows that it forms discrete nuclear foci in untreated cells, as well as upon exposure to DNA-damaging agents. As expected, these foci often co-localizing (magenta color) or in close proximity to the CPD foci, while at later time points, Polη foci were clearly separated from CPDs. Unlike PCNA^mUb, the intensity of the Polη foci increased immediately following UV irradiation, but it did not increase further with time, as determined by CellProfiler quantification (Figure S6F), while the CPD signal followed a trend similar to that observed in Figures 6 and S6E. Taken together, these observations suggest that upon UV irradiation, formation of PCNA^mUb and Polη foci is spatially distinct, suggesting a two-step process for TLS, such as activation at stalled forks (PCNA^mUb) and slow bypass by Polη (see discussion). Altogether, these results show that this protocol allows studying dynamics of PCNA^mUb and Polη foci in single cells, in relation to DNA lesions and DNA synthesis sites.

DISCUSSION

Failure to detect both endogenous PCNA^mUb and Y-family TLS pols in single cells has been a major hurdle to study TLS. This has been mainly due to lack of a specific antibody able to detect PCNA^mUb and probably to the low expression level of TLS pols. We have succeeded in detecting endogenous PCNA^mUb and TLS pols in single cells by both flow cytometry and immunofluorescence, suggesting that failure to detect them was not only a problem of abundance but also a matter of developing an opti-
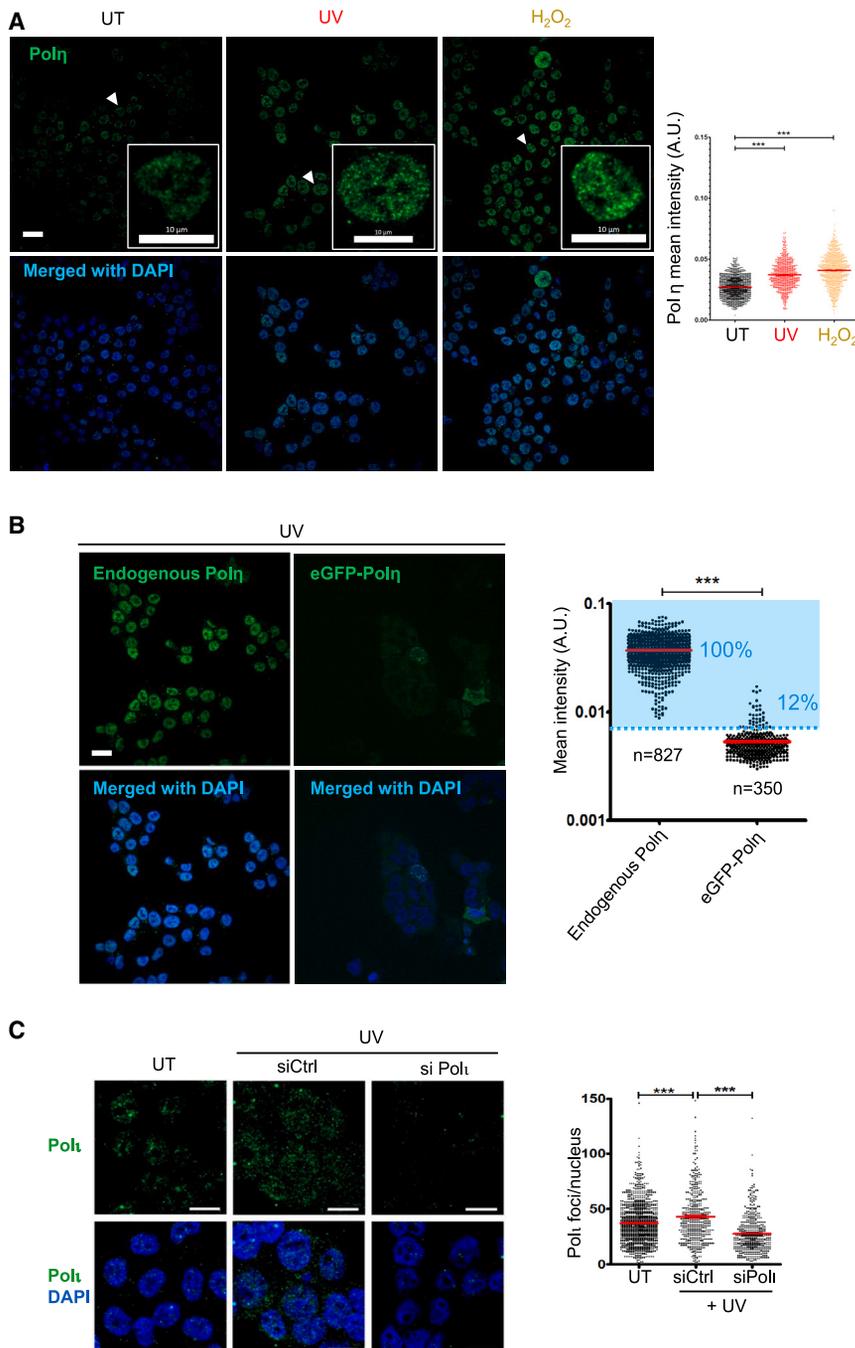
Figure 5. Detection of nuclear Polη in HCT116 cells treated with different DNA-damaging agents

(A) Left: detection of chromatin-bound Polη in HCT116 cells untreated (UT) or exposed to either 20 J/m² of UV-C light (UV), or 1 mM hydrogen peroxide (H₂O₂). Scale bar: 20 μm. Insets: magnification of the nuclei indicated by a white arrow. Right: quantification of Polη mean intensity in the indicated samples. A.U., arbitrary units. n = 3. Stars indicate significant differences. ***p < 0.001 (non-parametric Mann Whitney test). UV, n = 3; H₂O₂, n = 2.

(B) Left detection of either endogenous or ectopically expressed EGFP-Polη chromatin bound in HCT116 cells exposed to 20 J/m² of UV-C. Right: quantification of Polη foci intensity in the indicated samples. The percentage of Polη⁺ cells (blue gate) is indicated. Scale bar: 20 μm. Stars indicate significant differences. **p < 0.001 (non-parametric Mann Whitney test). n = 3.

(C) Left: detection of Polι by indirect immunofluorescence in HCT116 cells treated with either control siRNA (Ctrl) or Polι-specific siRNA, UT or exposed to 20 J/m² UV. Right: quantification of Polι foci per nucleus shown in (A). ***p < 0.001 (non-parametric Mann Whitney test). n = 2.
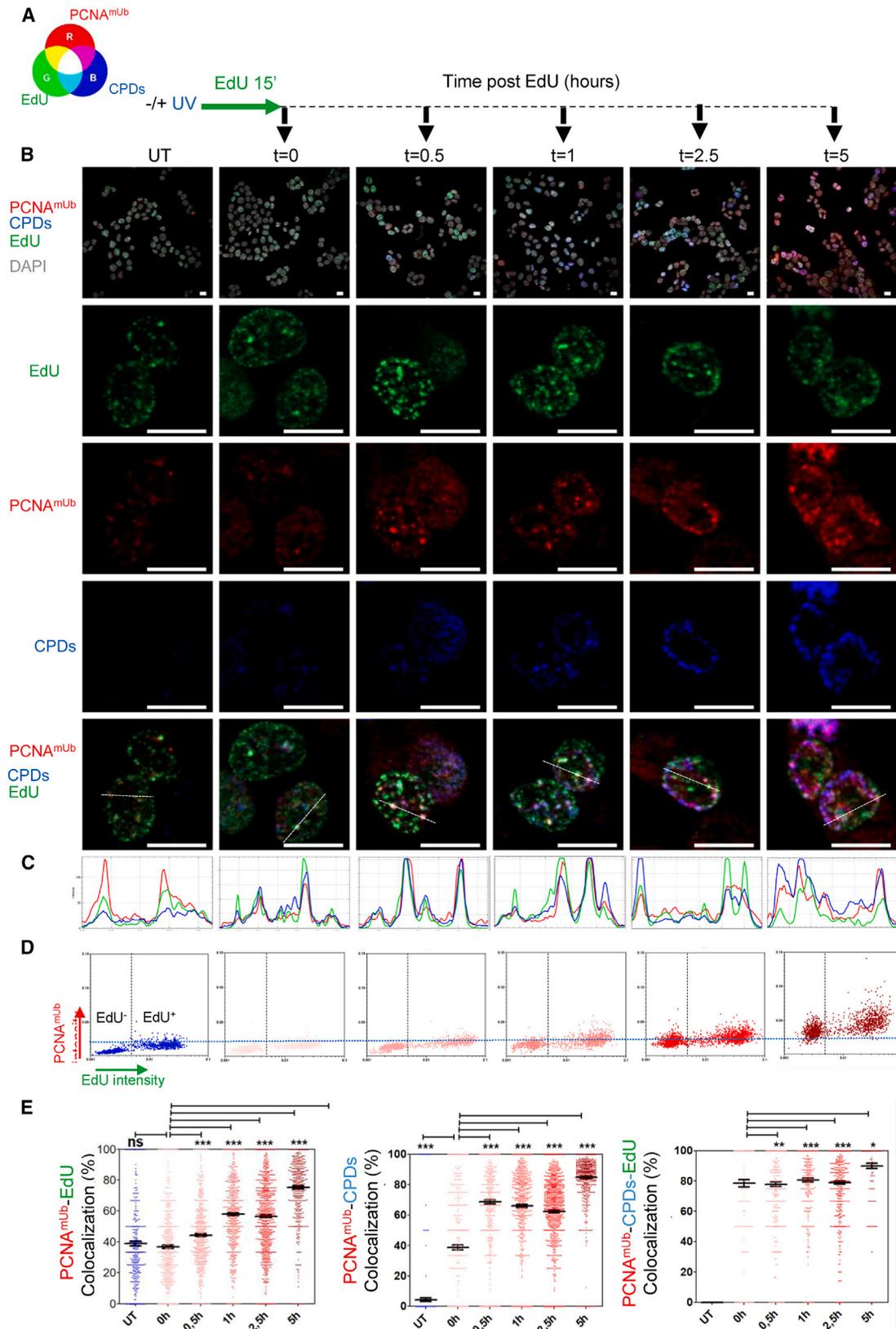
showing that Polη participates in DNA synthesis to assist the canonical replisome when encountering difficult-to-replicate DNA regions, such as repetitive DNA and common fragile sites.[17,34–36] Hence, it cannot be excluded that the observed differences may be due to ectopic overexpression of epitope-tagged Polη. Thus, detection of endogenous Polη with this protocol provides a more comprehensive picture compared with cells transfected with tagged versions of it. Importantly, Polη foci were found not co-localizing with sites of DNA synthesis (EdU) but were often in close proximity to them. This result is again different from previous observations using ectopically expressed GFP-Polη, in which co-localization was observed with sites of BrdU incorporation, although in as few as 15% of the cells,[13] which could be explained as forced recruitment of GFP-Polη upon overexpression.

were co-localized with PCNA, and to some extent with RPA, although they did not always overlap, while some other foci were clearly distinct from each other, suggesting ssDNA-dependent and -independent recruitment. The method described in this article also allowed detection of endogenous TLS Polη and Polι by immunofluorescence. Interestingly, in unperturbed cells, Polη formed discrete nuclear foci in virtually all cells, which is different from observations made using cells transfected with epitope-tagged Polη. The distribution of endogenous Polη as nuclear foci in all cells is consistent with several observations

A two-step process for TLS?

Current models in yeast suggest that following PCNA^mUb, TLS pols are immediately recruited to bypass the lesion and facilitate passage of the replication fork (TLS on the fly[37]), a situation that may be different in vertebrates. By investigating the dynamics of both PCNA^mUb and Polη by immunofluorescence in single HCT116 cells, during a time course of UV irradiation,

we have observed that PCNA^{mUb} co-localizes with UV-induced DNA lesions at sites of DNA synthesis (CPDs), while Polη did not, but was clearly located very close to EdU-positive sites. These results may suggest that in HCT116 cells, the signal required for TLS activation is generated at stalled replication forks, while Polη recruitment is a later event. A possible explanation of these observations is that the two processes, PCNA^{mUb} and Polη recruitment, are spatially distinct, similar to a recent observation reported in the yeast *S. cerevisiae*[38] and previous reports in vertebrate cells.[39–41] At late time points post-UV irradiation (5 h), Polη foci were close to EdU foci but clearly excluded from them, suggesting Polη recruitment at post-replicative gaps left behind the forks. Meanwhile, we cannot exclude that the Polη foci we observed correspond to TLS on the lagging strand and that TLS on the leading strand (on the fly) occurs too quick to be detected in fixed cells. Alternatively, on the leading strand, resumption of DNA synthesis downstream of a DNA lesion is assured by repriming by Primpol,[42] leaving gaps filled in post-replication in a Polη-dependent process. As a caveat, it cannot be excluded that the difference between PCNA^{mUb} and Polη localization may be due to the ability of Polη to bypass only CPDs, one of the two main lesions generated by UV-C irradiation. More detailed analysis of TLS dynamics in other cell lines and using super-resolution microscopy would be important to clarify this point. Isolated PCNA^{mUb} foci observed in untreated cells might represent sites of endogenous replication stress where replication forks stall frequently and therefore incorporate very few EdU. We have also been able to observe formation of discrete CPD foci in HCT116 cells, whose size increased with time following irradiation with UV-C light, suggesting clustering. These may represent sites of DNA repair in which NER factors may nucleate, thus opening the possibility to study NER factors recruitment to CPDs in single cells.

In conclusion, the procedures reported in this work now open a new avenue for the analysis of endogenous TLS pols, as well as of PCNA^{mUb} in virtually all cell types by either flow cytometry or immunofluorescence microscopy. This procedure might now also allow to study endogenous TLS activation in the context of somatic immunoglobulin gene hypermutation and maintenance of hematopoietic stem cells (Sale,[43] for review). In principle, the procedures described here will now make it possible to use TLS pols as well as PCNA^{mUb} as predictive markers for cancer resistance to therapeutic treatments (such as in BRCA-mutated and colon cancer[3,44] among others). Along this line, the use of PCNA^{mUb} and/or TLS pol staining could be useful to

set up screening strategies for the identification of chemical inhibitors, which could spin the development of TLS inhibitors. In this context, it is reasonable to expect the discovery of new synthetic lethal interactions that may be implemented to the current tool belt of chemo- or immunotherapeutic regimens used in cancer therapy.

Limitations of the study

The methods described in this article can, in principle, be applied to detect PCNA^{mUb} and TLS pols in any cell. A limitation in detecting these factors is their relative abundance, which depends upon the cell line, the proportion of S-phase cells, and the degree of endogenous replication stress. Another limitation is the availability of a suitable antibody to detect TLS pols, whose specificity must be first tested in cells depleted of the target. Insertion of a tag into the endogenous gene of interest by current CRISPR-Cas9 technology may help to circumvent this problem, although the possibility that the tag could change the affinity of the protein for chromatin has to be taken into account. We believe that this method will be very useful to study TLS dynamics at DNA replication forks stalled by diverse bulky DNA lesions and can be extended to TLS pols not included in our study.

STAR★METHODS

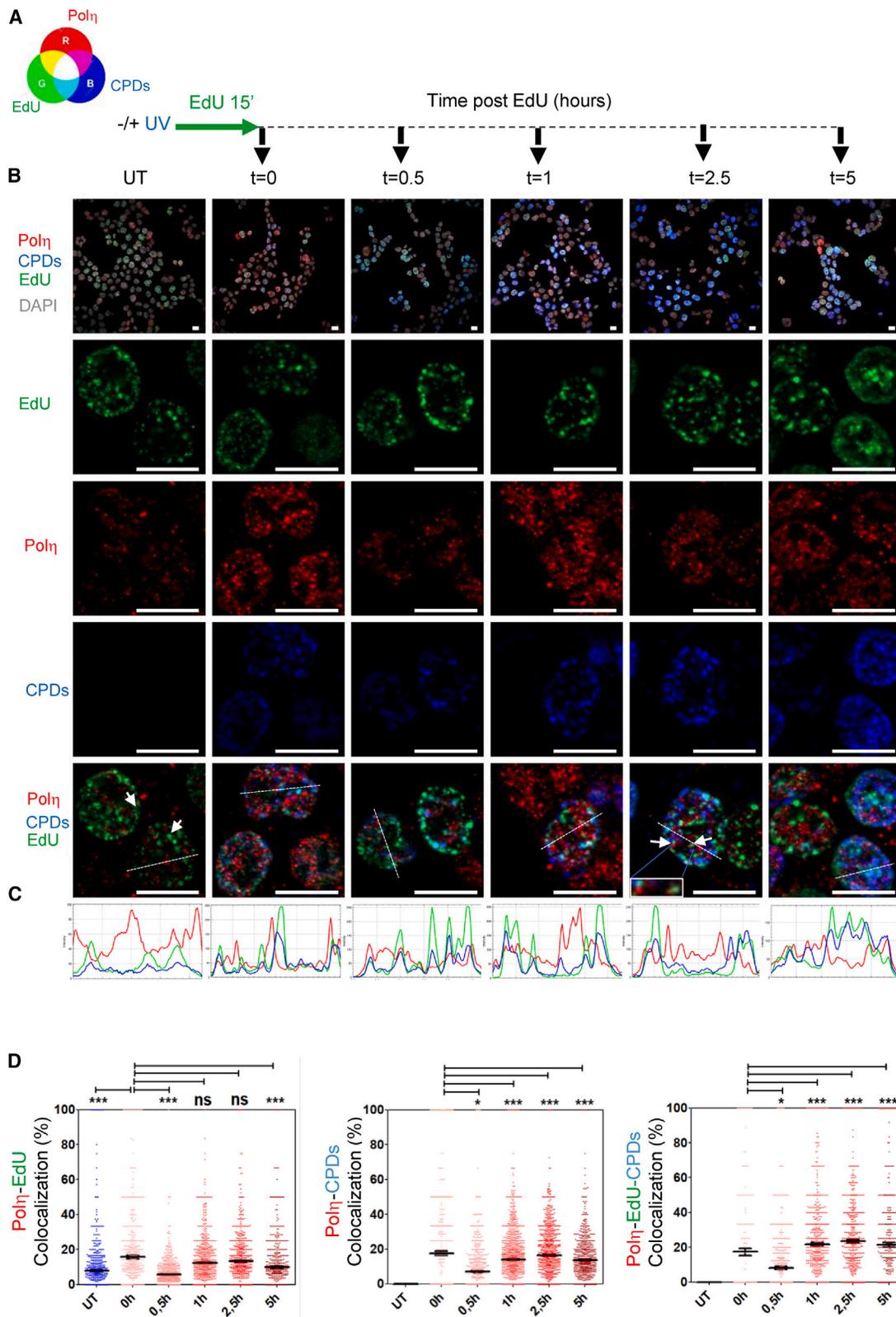Detailed methods are provided in the online version of this paper and include the following:

- KEY RESOURCES TABLE
- RESOURCE AVAILABILITY
  - Lead contact
  - Materials availability
  - Data and code availability
- EXPERIMENTAL MODEL AND SUBJECT DETAILS
  - Cell culture
- METHOD DETAILS
  - Samples preparation for flow cytometry
  - Western blotting
  - Immunofluorescence
  - Fluorescent labeling of ongoing DNA synthesis
- QUANTIFICATION AND STATISTICAL ANALYSIS

SUPPLEMENTAL INFORMATION

Supplemental information can be found online at https://doi.org/10.1016/j.crmeth.2023.100501.

Figure 6. Nuclear PCNA^{mUb} co-localization with UV-C-induced DNA lesions and sites of DNA synthesis in single cells

(A) Schematic drawing of the experimental procedure. A color table is included to facilitate the interpretation of the results.
(B) First row: wide-field images of HCT116 cells untreated (UT −UV) or exposed to UV-C (+UV), followed by pulse labeling with the nucleotide analog EdU. Antibodies were used to detect PCNA^{mUb} (red) and CPDs (blue), and EdU (green) was detected by click reaction (see STAR Methods) at the indicated times after UV-C exposure and viewed by indirect immunofluorescence. DNA was visualized with DAPI (gray). Other rows: magnification of single-cell nuclei from each wide field corresponding to each time point. Scale bar: 10 μm.
(C) Quantification of the relative intensity of the cross sections of the nuclei magnified in the top panel.
(D) Quantification of relative EdU and PCNA^{mUb} levels at the indicated time points post-UV irradiation. The black dashed line discriminates EdU$^−$ from EdU$^+$ cells (i.e., cells that were in S phase during the EdU pulse). The blue dashed line discriminates PCNA^{mUb}-negative from PCNA^{mUb}-positive cells (arbitrary gates). n = 2.
(E) Quantification of PCNA^{mUb}-EdU (left), PCNA^{mUb}-CPD (middle, and PCNA^{mUb}-CPD-EdU (right) co-localization. Stars indicate significant differences, *p < 0.05, ** p < 0.01, ***p < 0.001, ns, non-significant (non-parametric Mann Whitney test).

(legend on next page)

REFERENCES

1. Powers, K.T., and Washington, M.T. (2018). Eukaryotic translesion synthesis: choosing the right tool for the job. DNA Repair *71*, 127–134. https://doi.org/10.1016/j.dnarep.2018.08.016.

2. Nayak, S., Calvo, J.A., and Cantor, S.B. (2021). Targeting translesion synthesis (TLS) to expose replication gaps, a unique cancer vulnerability. Expert Opin. Ther. Targets *25*, 27–36. https://doi.org/10.1080/14728222.2021.1864321.

3. Russo, M., Crisafulli, G., Sogari, A., Reilly, N.M., Arena, S., Lamba, S., Bartolini, A., Amodio, V., Magrì, A., Novara, L., et al. (2019). Adaptive mutability of colorectal cancers in response to targeted therapies. Science *366*, 1473–1480. https://doi.org/10.1126/science.aav4474.

4. Kannouche, P.L., Wing, J., and Lehmann, A.R. (2004). Interaction of human DNA polymerase eta with monoubiquitinated PCNA: a possible mechanism for the polymerase switch in response to DNA damage. Mol. Cell *14*, 491–500.

5. Watanabe, K., Tateishi, S., Kawasuji, M., Tsurimoto, T., Inoue, H., and Yamaizumi, M. (2004). Rad18 guides poleta to replication stalling sites through physical interaction and PCNA monoubiquitination. EMBO J. *23*, 3886–3896.

6. Byun, T.S., Pacek, M., Yee, M.C., Walter, J.C., and Cimprich, K.A. (2005). Functional uncoupling of MCM helicase and DNA polymerase activities activates the ATR-dependent checkpoint. Genes Dev. *19*, 1040–1052.

7. Chang, D.J., Lupardus, P.J., and Cimprich, K.A. (2006). Monoubiquitination of proliferating cell nuclear antigen induced by stalled replication requires uncoupling of DNA polymerase and mini-chromosome maintenance helicase activities. J. Biol. Chem. *281*, 32081–32088. https://doi.org/10.1074/jbc.M606799200.

8. Batters, C., Zhu, H., and Sale, J.E. (2010). Visualisation of PCNA monoubiquitination in vivo by single pass spectral imaging FRET microscopy. PLoS One *5*, e9008. https://doi.org/10.1371/journal.pone.0009008.

9. Tissier, A., Kannouche, P., Reck, M.P., Lehmann, A.R., Fuchs, R.P.P., and Cordonnier, A. (2004). Co-localization in replication foci and interaction of human Y-family members, DNA polymerase pol eta and REVI protein. DNA Repair *3*, 1503–1514. https://doi.org/10.1016/j.dnarep.2004.06.015.

10. Bergoglio, V., Bavoux, C., Verbiest, V., Hoffmann, J.S., and Cazaux, C. (2002). Localisation of human DNA polymerase kappa to replication foci. J. Cell Sci. *115*, 4413–4418.

11. Bi, X., Slater, D.M., Ohmori, H., and Vaziri, C. (2005). DNA polymerase kappa is specifically required for recovery from the benzo[a]pyrene-dihydrodiol epoxide (BPDE)-induced S-phase checkpoint. J. Biol. Chem. *280*, 22343–22355. https://doi.org/10.1074/jbc.M501562200.

12. Kannouche, P., Fernández de Henestrosa, A.R., Coull, B., Vidal, A.E., Gray, C., Zicha, D., Woodgate, R., and Lehmann, A.R. (2003). Localization of DNA polymerases eta and iota to the replication machinery is tightly coordinated in human cells. EMBO J. *22*, 1223–1233. https://doi.org/10.1093/emboj/cdf618.

13. Kannouche, P., Broughton, B.C., Volker, M., Hanaoka, F., Mullenders, L.H., and Lehmann, A.R. (2001). Domain structure, localization, and function of DNA polymerase eta, defective in xeroderma pigmentosum variant cells. Genes Dev. *15*, 158–172.

14. Forment, J.V., Walker, R.V., and Jackson, S.P. (2012). A high-throughput, flow cytometry-based method to quantify DNA-end resection in mammalian cells. Cytometry A. *81*, 922–928. https://doi.org/10.1002/cyto.a.22155.

15. Thakar, T., Leung, W., Nicolae, C.M., Clements, K.E., Shen, B., Bielinsky, A.-K., and Moldovan, G.-L. (2020). Ubiquitinated-PCNA protects replication forks from DNA2-mediated degradation by regulating Okazaki fragment maturation and chromatin assembly. Nat. Commun. *11*, 2147. https://doi.org/10.1038/s41467-020-16096-w.

16. Swain, U., Friedlander, G., Sehrawat, U., Sarusi-Portuguez, A., Rotkopf, R., Ebert, C., Paz-Elizur, T., Dikstein, R., Carell, T., Geacintov, N.E., et al. (2021). TENT4A non-canonical poly(A) polymerase regulates DNA-damage tolerance via multiple pathways that are mutated in endometrial cancer. Int. J. Mol. Sci. *22*, 6957. https://doi.org/10.3390/ijms22136957.

17. Despras, E., Sittewelle, M., Pouvelle, C., Delrieu, N., Cordonnier, A.M., and Kannouche, P.L. (2016). Rad18-dependent SUMOylation of human specialized DNA polymerase eta is required to prevent under-replicated DNA. Nat. Commun. *7*, 13326. https://doi.org/10.1038/ncomms13326.

18. Recolin, B., van der Laan, S., Tsanov, N., and Maiorano, D. (2014). Molecular mechanisms of DNA replication checkpoint activation. Genes *5*, 147–175. https://doi.org/10.3390/genes5010147.

Figure 7. Nuclear Polη co-localization with UV-C-induced DNA lesions and sites of DNA synthesis by immunofluorescence in single cells
(A) Schematic drawing of the experimental procedure. A color table is included to facilitate the interpretation of the results.
(B) First row: wide-field images of HCT116 cells untreated (UT −UV) or exposed to UV-C light (+UV), followed by pulse labeling with the nucleotide analog EdU. Antibodies were used to detect Polη (red) and CPDs (blue), and EdU (green) was detected by click reaction at the indicated times after UV-C exposure and viewed by indirect immunofluorescence. DNA was visualized with DAPI (gray). Other rows: magnification of nuclei of single cells from each wide field corresponding to each time point. Scale bar: 10 μm.
(C) Quantification of the relative intensity of the cross-sections of the nuclei magnified in the top panel.
(D) Quantification of Polη-EdU (left), Polη-CPD (middle), and Polη-CPD-EdU (right) co-localization. Stars indicate significant differences, *p < 0.05; ***p < 0.001; ns, non-significant (non-parametric Mann Whitney test).

19. Toledo, L.I., Altmeyer, M., Rask, M.B., Lukas, C., Larsen, D.H., Povlsen, L.K., Bekker-Jensen, S., Mailand, N., Bartek, J., and Lukas, J. (2013). ATR prohibits replication catastrophe by preventing global exhaustion of RPA. Cell 155, 1088–1103. https://doi.org/10.1016/j.cell.2013.10.043.

20. Egger, T., Aze, A., and Maiorano, D. (2023). Protocol to analyze endogenous translesion DNA synthesis in single mammalian cells. STAR Protocols. https://doi.org/10.1016/j.xpro.2023.102361.

21. Terai, K., Abbas, T., Jazaeri, A.A., and Dutta, A. (2010). CRL4(Cdt2) E3 ubiquitin ligase monoubiquitinates PCNA to promote translesion DNA synthesis. Mol. Cell 37, 143–149. https://doi.org/10.1016/j.molcel.2009.12.018.

22. Masutani, C., Kusumoto, R., Yamada, A., Dohmae, N., Yokoi, M., Yuasa, M., Araki, M., Iwai, S., Takio, K., and Hanaoka, F. (1999). The XPV (xeroderma pigmentosum variant) gene encodes human DNA polymerase eta. Nature 399, 700–704. https://doi.org/10.1038/21447.

23. Somyajit, K., Spies, J., Coscia, F., Kirik, U., Rask, M.-B., Lee, J.-H., Neelsen, K.J., Mund, A., Jensen, L.J., Paull, T.T., et al. (2021). Homology-directed repair protects the replicating genome from metabolic assaults. Dev. Cell 56, 461–477.e7. https://doi.org/10.1016/j.devcel.2021.01.011.

24. Andersen, P.L., Xu, F., Ziola, B., McGregor, W.G., and Xiao, W. (2011). Sequential assembly of translesion DNA polymerases at UV-induced DNA damage sites. MBoC 22, 2373–2383. https://doi.org/10.1091/mbc.e10-12-0938.

25. Tsanov, N., Kermi, C., Coulombe, P., Van der Laan, S., Hodroj, D., and Maiorano, D. (2014). PIP degron proteins, substrates of CRL4Cdt2, and not PIP boxes, interfere with DNA polymerase η and κ focus formation on UV damage. Nucleic Acids Res. 42, 3692–3706. https://doi.org/10.1093/nar/gkt1400.

26. Jagirdar, K., Yin, K., Harrison, M., Lim, W., Muscat, G.E.O., Sturm, R.A., and Smith, A.G. (2013). The NR4A2 nuclear receptor is recruited to novel nuclear foci in response to UV irradiation and participates in nucleotide excision repair. PLoS One 8, e78075. https://doi.org/10.1371/journal.pone.0078075.

27. Zheng, Y., Pao, A., Adair, G.M., and Tang, M. (2001). Cyclobutane pyrimidine dimers and bulky chemical DNA adducts are efficiently repaired in both strands of either a transcriptionally active or promoter-deleted APRT gene. J. Biol. Chem. 276, 16786–16796. https://doi.org/10.1074/jbc.M010973200.

28. Yang, Y., Durando, M., Smith-Roe, S.L., Sproul, C., Greenwalt, A.M., Kaufmann, W., Oh, S., Hendrickson, E.A., and Vaziri, C. (2013). Cell cycle stage-specific roles of Rad18 in tolerance and repair of oxidative DNA damage. Nucleic Acids Res. 41, 2296–2312. https://doi.org/10.1093/nar/gks1325.

29. Zlatanou, A., Despras, E., Braz-Petta, T., Boubakour-Azzouz, I., Pouvelle, C., Stewart, G.S., Nakajima, S., Yasui, A., Ishchenko, A.A., and Kannouche, P.L. (2011). The hMsh2-hMsh6 complex acts in concert with monoubiquitinated PCNA and Pol eta in response to oxidative DNA damage in human cells. Mol. Cell 43, 649–662. https://doi.org/10.1016/j.molcel.2011.06.023.

30. Ogi, T., Limsirichaikul, S., Overmeer, R.M., Volker, M., Takenaka, K., Cloney, R., Nakazawa, Y., Niimi, A., Miki, Y., Jaspers, N.G., et al. (2010). Three DNA polymerases, recruited by different mechanisms, carry out NER repair synthesis in human cells. Mol. Cell 37, 714–727. https://doi.org/10.1016/j.molcel.2010.02.009.

31. Nakajima, S., Lan, L., Kanno, S.i., Usami, N., Kobayashi, K., Mori, M., Shiomi, T., and Yasui, A. (2006). Replication-dependent and -independent responses of RAD18 to DNA damage in human cells. J. Biol. Chem. 281, 34687–34695. https://doi.org/10.1074/jbc.M605545200.

32. Karras, G.I., and Jentsch, S. (2010). The RAD6 DNA damage tolerance pathway operates uncoupled from the replication fork and is functional beyond S phase. Cell 141, 255–267. https://doi.org/10.1016/j.cell.2010.02.028.

33. Shibutani, S., Takeshita, M., and Grollman, A.P. (1991). Insertion of specific bases during DNA synthesis past the oxidation-damaged base 8-oxodG. Nature 349, 431–434. https://doi.org/10.1038/349431a0.

34. Bergoglio, V., Boyer, A.S., Walsh, E., Naim, V., Legube, G., Lee, M.Y.W.T., Rey, L., Rosselli, F., Cazaux, C., Eckert, K.A., et al. (2013). DNA synthesis by Pol eta promotes fragile site stability by preventing under-replicated DNA in mitosis. J. Cell Biol. 201, 395–408. https://doi.org/10.1083/jcb.201207066.

35. Twayana, S., Bacolla, A., Barreto-Galvez, A., De-Paula, R.B., Drosopoulos, W.C., Kosiyatrakul, S.T., Bouhassira, E.E., Tainer, J.A., Madireddy, A., and Schildkraut, C.L. (2021). Translesion polymerase eta both facilitates DNA replication and promotes increased human genetic variation at common fragile sites. Proc. Natl. Acad. Sci. USA 118, e2106477118. https://doi.org/10.1073/pnas.2106477118.

36. Lo Furno, E., Busseau, I., Aze, A., Lorenzi, C., Saghira, C., Danzi, M.C., Zuchner, S., and Maiorano, D. (2022). Translesion DNA synthesis-driven mutagenesis in very early embryogenesis of fast cleaving embryos. Nucleic Acids Res. 50, 885–898. https://doi.org/10.1093/nar/gkab1223.

37. Guilliam, T.A., and Yeeles, J.T.P. (2020). Reconstitution of translesion synthesis reveals a mechanism of eukaryotic DNA replication restart. Nat. Struct. Mol. Biol. 27, 450–460. https://doi.org/10.1038/s41594-020-0418-4.

38. Wong, R.P., García-Rodríguez, N., Zilio, N., Hanulová, M., and Ulrich, H.D. (2020). Processing of DNA polymerase-blocking lesions during genome replication is spatially and temporally segregated from replication forks. Mol. Cell 77, 3–16.e4. https://doi.org/10.1016/j.molcel.2019.09.015.

39. Edmunds, C.E., Simpson, L.J., and Sale, J.E. (2008). PCNA ubiquitination and REV1 define temporally distinct mechanisms for controlling translesion synthesis in the avian cell line DT40. Mol. Cell 30, 519–529. https://doi.org/10.1016/j.molcel.2008.03.024.

40. Diamant, N., Hendel, A., Vered, I., Carell, T., Reissner, T., de Wind, N., Geacinov, N., and Livneh, Z. (2012). DNA damage bypass operates in the S and G2 phases of the cell cycle and exhibits differential mutagenicity. Nucleic Acids Res. 40, 170–180. https://doi.org/10.1093/nar/gkr596.

41. Tirman, S., Quinet, A., Wood, M., Meroni, A., Cybulla, E., Jackson, J., Pegoraro, S., Simoneau, A., Zou, L., and Vindigni, A. (2021). Temporally distinct post-replicative repair mechanisms fill PRIMPOL-dependent ssDNA gaps in human cells. Mol. Cell 81, 4026–4040.e8. https://doi.org/10.1016/j.molcel.2021.09.013.

42. Cortez, D. (2019). Replication-coupled DNA repair. Mol. Cell 74, 866–876. https://doi.org/10.1016/j.molcel.2019.04.027.

43. Sale, J.E. (2013). Translesion DNA synthesis and mutagenesis in eukaryotes. Cold Spring Harb. Perspect. Biol. 5, a012708. https://doi.org/10.1101/cshperspect.a012708.

44. Nayak, S., Calvo, J.A., Cong, K., Peng, M., Berthiaume, E., Jackson, J., Zaino, A.M., Vindigni, A., Hadden, M.K., and Cantor, S.B. (2020). Inhibition of the translesion synthesis polymerase REV1 exploits replication gaps as a cancer vulnerability. Sci. Adv. 6, eaaz7808. https://doi.org/10.1126/sciadv.aaz7808.

45. Langerak, P., Nygren, A.O.H., Krijger, P.H.L., van den Berk, P.C.M., and Jacobs, H. (2007). A/T mutagenesis in hypermutated immunoglobulin genes strongly depends on PCNAK164 modification. J. Exp. Med. 204, 1989–1998. https://doi.org/10.1084/jem.20070902.

46. Durando, M., Tateishi, S., and Vaziri, C. (2013). A non-catalytic role of DNA polymerase eta in recruiting Rad18 and promoting PCNA monoubiquitination at stalled replication forks. Nucleic Acids Res. 41, 3079–3093. https://doi.org/10.1093/nar/gkt016.

47. Bétous, R., Pillaire, M.J., Pierini, L., van der Laan, S., Recolin, B., Ohl-Séguy, E., Guo, C., Niimi, N., Grúz, P., Nohmi, T., et al. (2013). DNA

polymerase kappa-dependent DNA synthesis at stalled replication forks is important for CHK1 activation. EMBO J. *32*, 2172–2185. https://doi.org/10.1038/emboj.2013.148.

48. Kermi, C., Prieto, S., van der Laan, S., Tsanov, N., Recolin, B., Uro-Coste, E., Delisle, M.B., and Maiorano, D. (2015). RAD18 is a maternal limiting factor silencing the UV-dependent DNA damage checkpoint in Xenopus embryos. Dev. Cell *34*, 364–372. https://doi.org/10.1016/j.devcel.2015.06.002.

49. Stirling, D.R., Swain-Bowden, M.J., Lucas, A.M., Carpenter, A.E., Cimini, B.A., and Goodman, A. (2021). CellProfiler 4: improvements in speed, utility and usability. BMC Bioinf. *22*, 433. https://doi.org/10.1186/s12859-021-04344-9.

Cell Reports Methods
Article

STAR★METHODS

KEY RESOURCES TABLE

REAGENT or RESOURCE	SOURCE	IDENTIFIER
Antibodies		
Ubiquityl-PCNA (Lys164)	Cell Signaling Technology	RRID:AB_2798219
PCNA	Millipore	RRID:AB_11203836
α-tubulin	Sigma-Aldrich	RRID:AB_477583
Rad18	Abcam	RRID:AB_1603946
CHK1	Santa Cruz Biotechnology	RRID:AB_627257
CHK1^{pS345}	Cell Signaling Technology	RRID:AB_331212
γH2AX	Cell Signaling Technology	RRID:AB_2118009
H2AX	Cell Signaling Technology	RRID:AB_10694556
Polη	Abcam	RRID:AB_2756352
Polκ	Atlas Antibodies	RRID:AB_2668606
Polι	Proteintech	RRID:AB_2167009
RPA	Abcam	RRID:AB_302873
CPDs	Cosmo Bio	RRID:AB_1962813
USP1	Proteintech	RRID:AB_2214314
Histone H2B	Abcam	RRID:AB_302612
Goat Anti-Rabbit Alexa 488	Thermo Fisher Scientific	RRID:AB_2576217
Goat Anti-Rabbit Alexa 568	Thermo Fisher Scientific	RRID:AB_10563566
Goat anti-Mouse Alexa 660	Thermo Fisher Scientific	RRID:AB_2535722
Goat anti-Mouse Alexa 660	Thermo Fisher Scientific	RRID:AB_2535722
Goat anti-Rabbit HRP	Cell Signaling Technology	RRID:AB_2099233
Goat anti-Mouse HRP	Cell Signaling Technology	RRID:AB_330924
Chemicals, peptides and recombinant proteins		
Camptothecin	Sigma-Aldrich	C9911
Cisplatin	Sigma-Aldrich	P4394
DAPI	Sigma-Aldrich	D9542
Formaldehyde	Thermo Fisher	28908
Hydrogen Peroxyde	Sigma-Aldrich	216763
Sodium fluoride	Sigma-Aldrich	201154
β-Glycerophosphate	Sigma-Aldrich	G9422
Halt Proteases and Phosphatases inhibitors	Thermo Fisher Scientific	78440
Perm/Wash buffer	BD biosciences	554723
Prolong Diamond AntiFade	Thermo Fisher	P36961
RNAse A	EMD Millipore	70856
Benzonase	Sigma-Aldrich	E1014-5KU
BSA	Sigma-Aldrich	A2153
Critical commercial assays		
BCA Protein Assay Kit	Thermo Fisher Scientific	23225
Click-iT EdU 488	Thermo Fisher Scientific	C10337
ECL Crescendo	Millipore	WBLUR0500
Experimental models: Cell lines		
HCT166	ATCC	CCL-247
NCI-H1299	ATCC	CRL-5803
HEK293T	ATCC	CRL-3216

(Continued on next page)

Continued		
REAGENT or RESOURCE	SOURCE	IDENTIFIER
T98G	ATCC	CRL-1690
XP30RO	Masutani et al.[22]	N/A
XP30RO:Polη	Kannouche et al.[13]	N/A
XP30RO:GFP-Polη	Kannouche et al. [13]	N/A
MEFs wild-type	Langerak et al.[45]	N/A
MEFs *pcna^K164R*	Langerak al.[45]	N/A
Oligonucleotides		
Control siRNA (Luciferase)	5′-CACGUACGCGG AAUACUUCGGATT-3′	N/A
Polη siRNA	Durando et al.[46]	N/A
Polι siRNA	Somyajit et al.[23]	N/A
Polκ siRNA	Bétous et al.[47]	N/A
Rad18 siRNA	Kermi et al.[48]	N/A
Recombinant DNA		
pEGFP:Polη	Kannouche et al.[13]	N/A
pCDNA3-HA-FLAG*pcna^K164R*	This paper	N/A
Software and algorithms		
Cell Profiler 4.2.1	Stirling et al.[49]	N/A
Kaluza	Beckman Coulter	N/A
Zen Blue	Zeiss	N/A
Prism	GraphPad	N/A
Other		
4–15% Criterion™ TGX™ Precast Midi Protein Gel,	BioRad	5671085
Tris/Glycin Buffer	BioRad	1610771EDU
Trans-Blot Turbo Transfer System	BioRad	1704150
ChemiDoc	Biorad	N/A
Poly-D-Lysine	Gibco	A38904-01

RESOURCE AVAILABILITY

Lead contact
Further information and requests for resources and reagents should be directed to and will be fulfilled by the lead contact, Domenico Maiorano (domenico.maiorano@igh.cnrs.fr).

Materials availability
All unique/stable reagents generated in this study are available from the lead contact upon reasonable request with a completed Materials Transfer Agreement.

Data and code availability
- All data reported in this paper will be shared by the lead contact upon request.
- This paper does not report original code.
- Any additional information required to reanalyze the data reported in this paper is available from the lead contact upon request.

EXPERIMENTAL MODEL AND SUBJECT DETAILS

Cell culture
Cells were cultured in DMEM-GlutaMAX (ThermoFisher #10566-016) supplemented with 10% FBS (Eurobio, #CVFSVF00-01) at 37°C, 5% CO$_2$. Cells were maintained in exponential growth phase and passaged 2–3 times a week for 20–25 passages before being discarded. Cells were tested negative for mycoplasma at thawing. Before any drug treatments, cells were seeded at an equivalent

density and allowed to attach overnight. For the UV irradiation, cells were washed in PBS and exposed to 20 J/m^2 of UV-C light using a Stratalinker (Stratagene) and released in fresh medium for 5 h (unless stated otherwise) before being processed for western blot, immunofluorescence or flow cytometry, as described below. For cisplatin and camptothecin treatments, cells were exposed respectively to either 30 μM or 1 μM for 5 h. For the hydrogen peroxide treatment, cells were exposed to 1 mM for 30 min. Transfection of HEK293T cells with pCDNA3-HA-flag-*pcna*^{K164R} was performed using Lipofectamine™ 2000 (Invitrogen, 11668027) according to manufacturer instructions. For Polι and Polη silencing by siRNA, HCT116 cells were transfected with Lipofectamine RNAi MAX (Thermofisher Scientific, 13778100).

METHOD DETAILS

Samples preparation for flow cytometry

1×10^6 cells were seeded in 6-well plates. After drug treatments, cells were trypsinized, washed with ice-cold PBS and pelleted at 400 x *g* for 5 min. The extraction, fixation and immunodetection of targets were performed with optimized revisions of a previous protocol.[14] The extraction was performed for 5–10 min on ice in 100 μL of a PBS-0,2 to 0.5% Triton X-100 buffer (depending on the target, see Figure 2E and Egger et al.[20]), and stopped by addition of 500 μL of PBS containing 1 mg/mL BSA. Nuclei were pelleted at 500 x *g* for 5 min and fixed by gentle resuspension in PBS containing either 2% formaldehyde for 30 min at room temperature or in pre-chilled PBS containing 90% methanol, for 10 min at −20°C, depending on the target proteins to be detected (see Figure 2E). The fixation was stopped with 1 mL 1 x Perm/Wash buffer (BD Biocience). Nuclei were pelleted at 750 x *g* for 5 min and washed in 1 x Perm/Wash buffer once. Target proteins were detected using the indicated antibodies diluted at 1/100 in 50 μL of 1 x Perm/Wash buffer overnight at 4°C in gentle rotation motion. Nuclei were washed by adding 500 μL of 1 x Perm/Wash buffer and pelleted at 750 x *g* for 5min. Nuclei were then incubated 1 h at RT with the indicated secondary antibodies, diluted at 1/250 in 1 x Perm/Wash buffer before being washed by the addition of 500 μL of 1 x Perm/Wash buffer. Nuclei were pelleted at 750 x *g* for 5 min and dissolved in 300 μL of PBS, 1 mg/mL BSA, 1 μg/mL DAPI, 100 μg/mL RNase A. Preparations were incubated at 37°C for 30 min before being analyzed on a Gallios Flow Cytometer (Beckman Coulter). Forward Scatter/Side Scatter-based debris exclusion was set up, and the doublets were excluded using the DAPI Height/DAPI Area graphs. 20,000 cells were analyzed per sample on the Kaluza dedicated software.

Western blotting

Cells were cultured in 6-well plates. Typically, 0,5-1 X 10^6 cells were seeded per well. At 70–80% confluence, cells were harvested by trypsinization, rinsed in ice-cold 1 x PBS. For whole cell extracts (WCE), proteins were extracted in 100μL of lysis buffer (10 mM HEPES-KOH pH 7.5, 200 mM NaCl, 0.5% NP-40, 2 mM MgCl$_2$, 1 mM DTT, 1 mM PMSF) containing 1 mM sodium fluoride and 1 mM β-Glycerophosphate, completed with 1/1000 Benzonase nuclease. Cells were lysed in lysis buffer for 15 min at room temperature (with agitation, 1000 rpm). Debris were pelleted at 13,000 x *g*, 20 min, 4°C. Proteins were quantified using the BCA Protein Assay Kit.

For cell fractionation (chromatin/soluble), cells were lysed in 100 μL of PBS-0.2% Triton X-100 containing Halt Proteases and Phosphatases inhibitors for 10 min on ice. The chromatin fractions were then pelleted (3200 rpm, 3 min), while the supernatants were isolated (soluble fractions) and quantified with the BCA Protein Assay Kit. Laemmli buffer was added to the soluble fraction to a final concentration of 1 x. The chromatin pellets were then washed in the same lysis buffer for 10 min on ice before being pelleted again (3200 rpm, 3 min). Supernatants were discarded and chromatin pellets were dissolved in 100 μL of lysis buffer containing 1 x Laemmli buffer.

In both cases (WCE and cell fractionation), equivalent amounts of proteins were loaded in 4–15% Criterion™ TGX™ Precast Midi Protein Gel, 26 well. Gels were run at 150 V in 1 x Tris/Glycin Buffer. Proteins were transferred onto 0.2 μm nitrocellulose membranes (BioRad, #1704271) using the Trans-Blot Turbo Transfer System set on the mixed molecular weight program. Total proteins were stained with Ponceau S and membranes were saturated in TBS-0.1% Tween 20, 5% non-fat dry milk for 1 h at room temperature. Target proteins were immunodetected overnight at 4°C in TBS-0.1% Tween 20, 5% BSA. Membranes were rinsed 3 × 10 min in TBS-0.1% Tween 20 and incubated for 1 h at room temperature in a TBS-0.1% Tween 20, 5% non-fat dry milk containing the HRP-conjugated secondary antibodies diluted at 1/3000. Membranes were rinsed 3 × 10min in TBS-0.1% Tween 20 and revealed using ECL Crescendo using a ChemiDoc device.

Immunofluorescence

Cells were grown on Poly-D-Lysine-coated 14 mm glass coverslips in 6-well plates. Cell were rinsed in PBS and the cytoplasm was extracted with PBS-0.2% Triton X-100 solution on ice for 3 to 10 min and Egger et al.[20]. Addition of 200 mM sucrose to the extraction buffer improves TLS pols detection. Nuclei were then immediately fixed in either 2% formaldehyde (room temperature for 30min) or by adding 90% methanol in PBS dropwise (−20°C, 10 min), depending on the target proteins to be detected (See Figure 2E). Nuclei were rinsed in PBS containing 1 mg/mL BSA. Nuclei were then saturated for 1 h in 1 x Perm/Wash buffer. Target proteins were detected using the indicated antibodies diluted at 1/100 in 1 x Perm/Wash buffer overnight at 4°C in a humid chamber. Coverslips were rinsed 3 × 5 min in 1 x Perm/Wash buffer and incubated 1h at room temperature with secondary antibodies (Alexa Fluor), diluted at 1/250 in 1 x Perm/Wash buffer. Coverslips were rinsed 3 × 5min in 1 x Perm/Wash buffer and nuclei were counterstained with DAPI (1 μg/mL) for 5 min at room temperature. Coverslips were mounted in Prolong Diamond AntiFade and observed on a Zeiss Axio

Imager with a X63 objective and the Apotome engaged. Pictures were saved and processed using the Zen Blue dedicated software, with the same exposure times. Equivalent display settings were used in the related panels. The cross sections (line scan intensity profile) were performed using ImageJ.

Fluorescent labeling of ongoing DNA synthesis

EdU detection by Click reaction (Click-iT EdU 488 Thermo Fisher Scientific, C10337) was performed as recommended by the manufacturer.

QUANTIFICATION AND STATISTICAL ANALYSIS

The apotome images were converted (Aptome RAW convert, Zen Blue) and imported into Cell Profiler 4.2.1. The Metadata of each fluorescent channel were extracted and nuclei were identified (Identify Primary Objects: Blue channel, Size 70–200 pixels, border events exclusion = yes, Threshold strategy: Global, Thresholding method: Manual, Threshold: 0.01, Threshold smoothing scale: 1.2, distinguish clumped objects: Shape, draw dividing lines: propagate). The mean intensity in the green and red targets were computed for each nucleus (previously detected) and presented using GraphPad Prism 5. For foci counting, complementary Identify Primary Objects steps were added for each target to be quantified. (Identify Primary Objects: Green/Red channels, Size 2–20 pixels, border events exclusion = yes, Threshold strategy: Global, Thresholding method: Otsu). Foci were related to their respective parent object (nuclei) and the number of foci in each nucleus was plotted using GraphPad Prism 5. The colocalization pipeline used to generate the graphs (Figures 6E and 7D) is available upon request. Briefly, it calculates the percentage of colocalizing foci per nucleus. Metadata (i.e. the conditions) were extracted based on the name of the Apotome RAW converted files (.czi, Zeiss, Zen Blue 2.3). Channels (Hoescht C = 0, Alexa Fluor 488 C = 1, AlexFluor 568 C = 2, Alexa Fluor 647 C = 3) were identified in the NamesAndTypes section. Automated nuclei detection and segmentation was performed using the IdentifyPrimaryObject function with the Otsu (Two classes) thresholding method. Nuclear foci of each target proteins were detected in a similar way, after an enhancement step (EnhanceOrSupressFeatures, speckles), using the manual thresholding method, before finally being related to their parent nucleus (RelatedObject function). Colocalizing objects were identified as the overlapping parts of different colors foci and related to their parent nuclei using the same strategy. The percentage of colocalizing foci per nucleus was then calculated as the ratio of the number of colocalized foci versus the total foci count of a defined color in individual nuclei, i.e:

$$\% \text{ of Color A}+, \text{ Color B foci} = \frac{(Color\ A+B)\ colocalized\ foci\ count}{Total\ color\ B\ foci\ count}, \text{ per nucleus}$$

Quality controls of nuclei segmentation and foci identification were systematically performed using the GrayToColor and OverlayOutlines functions, reconstructing all analyzed images and outlying idenftied nuclei and foci of each color.

Statistical analysis was performed on GraphPad Prism 5. For the Cell Profiler analyses, non-parametric Mann-Whitney tests were performed: *: $p < 0.05$; **: $p < 0.01$; ***: $p < 0.001$; ns, non-significant. "n" indicated in each figure legends refers to the number of times the experiment was replicated and data shown are representative of the "n" experiments performed with consistent and reproducible results.